

Entropic effect on the rate of dislocation nucleation

Seunghwa Ryu^{a,1}, Keonwook Kang^b, and Wei Cai^b

^aDepartment of Physics, and ^bDepartment of Mechanical Engineering, Stanford University, Stanford, CA 94305

Edited* by William D. Nix, Stanford University, Stanford, CA, and approved January 27, 2011 (received for review November 15, 2010)

Dislocation nucleation is essential to our understanding of plastic deformation, ductility, and mechanical strength of crystalline materials. Molecular dynamics simulation has played an important role in uncovering the fundamental mechanisms of dislocation nucleation, but its limited timescale remains a significant challenge for studying nucleation at experimentally relevant conditions. Here we show that dislocation nucleation rates can be accurately predicted over a wide range of conditions by determining the activation free energy from umbrella sampling. Our data reveal very large activation entropies, which contribute a multiplicative factor of many orders of magnitude to the nucleation rate. The activation entropy at constant strain is caused by thermal expansion, with negligible contribution from the vibrational entropy. The activation entropy at constant stress is significantly larger than that at constant strain, as a result of thermal softening. The large activation entropies are caused by anharmonic effects, showing the limitations of the harmonic approximation widely used for rate estimation in solids. Similar behaviors are expected to occur in other nucleation processes in solids.

Nucleation plays an important role in a wide range of physical, chemical, and biological processes (1–6). In the last two decades, the nucleation of dislocations in crystalline solids has attracted significant attention, not only for the reliability of microelectronic devices (7), but also as a responsible mechanism for incipient plasticity in nanomaterials (8–10) and nanoindentation (11–13). However, predicting the nucleation rate as a function of temperature and stress from fundamental physics is extremely difficult. Because the critical nucleus can be as small as a few lattice spacings, the applicability of continuum theory (14) becomes questionable. At the same time, the timescale of molecular dynamics (MD) simulations is about ten orders of magnitude smaller than the experimental timescale. Hence MD simulations of dislocation nucleation are limited to conditions at which the nucleation rate is extremely high (15, 16).

One way to predict the dislocation nucleation rate under common experimental loading rates (17) is to combine the transition state theory (TST) (5, 18) and the nudged elastic band (NEB) method (19). TST predicts that the nucleation rate per nucleation site in a crystal subjected to constant strain γ can be written as

$$I^{\text{TST}} = \nu_0 \exp \left[-\frac{F_c(T, \gamma)}{k_B T} \right], \quad [1]$$

where F_c is the activation free energy, T is temperature, and k_B is Boltzmann's constant. The frequency prefactor is $\nu_0 = k_B T/h$, where h is Planck's constant. Note that $F_c(T, \gamma) = E_c(\gamma) - TS_c(\gamma)$, where E_c and S_c are the activation energy and activation entropy, respectively. Here we assume the dependence of E_c and S_c on T is weak, which is later confirmed numerically for $T \leq 400$ K. For a crystal subjected to constant stress σ , $F_c(T, \gamma)$ in Eq. 1 should be replaced by the activation Gibbs free energy $G_c(T, \sigma) = H_c(\sigma) - TS_c(\sigma)$, where H_c is the activation enthalpy. Because the NEB method only computes the activation energy, the contribution of S_c is often ignored in rate estimates in solids. Recently, an approximation of $S_c(\sigma) = H_c(\sigma)/T_m$ is used (17), where T_m is the surface disordering temperature. This approximation was questioned by subsequent MD simulations (20). The magnitude of S_c remains unknown because none of the existing methods for

computing activation free energies (21–23) has been successfully applied to dislocation nucleation.

We successfully applied the umbrella sampling (21) method to compute the activation free energy for homogeneous and heterogeneous dislocation nucleation in copper. Based on this input, the nucleation rate is predicted using the Becker–Döring theory (24). Comparison with direct MD simulations at high stress confirms the accuracy of this approach. Both $F_c(T, \gamma)$ and $G_c(T, \sigma)$ show significant reduction with increasing T , corresponding to large activation entropies. For example, $S_c(\gamma = 0.092) = 9k_B$ and $S_c(\sigma = 2 \text{ GPa}) = 48k_B$ are observed in homogeneous nucleation. We found that $S_c(\gamma)$ is caused by the anharmonic effect of thermal expansion, with negligible contribution from the vibrational entropy. The large difference in the two activation entropies, $\Delta S_c \equiv S_c(\sigma) - S_c(\gamma)$, is caused by thermal softening, which is another anharmonic effect. Similar behaviors are expected to occur in other nucleation processes in solids.

For simplicity, we begin with the case of homogeneous dislocation nucleation in the bulk. Even though dislocations often nucleate heterogeneously at surfaces or internal interfaces, homogeneous nucleation is believed to occur in nanoindentation (11) and in a model of brittle–ductile transition (25). It also provides an upper bound to the ideal strength of the crystal. Our model system is a copper single crystal described by the embedded atom method (EAM) potential (26). As shown in Fig. 1A, the simulation cell is subjected to a pure shear stress along $[11\bar{2}]$. The dislocation to be nucleated lies on the (111) plane and has the Burgers vector of a Shockley partial (27), $\mathbf{b}_p = [11\bar{2}]/6$. Fig. 1B shows the shear stress strain relationship of the perfect crystal at different temperatures (before dislocation nucleation).

In this work, we predict the nucleation rate based on the Becker–Döring (BD) theory, which expresses the nucleation rate per nucleation site as

$$I^{\text{BD}} = f_c^+ \Gamma \exp \left[-\frac{F_c(T, \gamma)}{k_B T} \right], \quad [2]$$

where f_c^+ is the molecular attachment rate, and Γ is the Zeldovich factor (*Materials and Methods*). The BD theory and TST only differs in the frequency prefactor. Whereas TST neglects multiple recrossing over the saddle point by a single transition trajectory (5), the recrossing is accounted for in the BD theory through the Zeldovich factor.

First, we establish the validity of the BD theory for dislocation nucleation by comparing it against direct MD simulations at a relatively high stress $\sigma = 2.16$ GPa ($\gamma = 0.135$) at $T = 300$ K, which predicts $I^{\text{MD}} = 2.5 \times 10^8 \text{ s}^{-1}$ (*Materials and Methods*). The key input to the BD theory is the activation Helmholtz free energy $F_c(T, \gamma)$, which is computed by umbrella sampling. The

Author contributions: S.R. and W.C. designed research; S.R., K.K., and W.C. performed research; S.R. and K.K. contributed new reagents/analytic tools; S.R. and W.C. analyzed data; and S.R., K.K., and W.C. wrote the paper.

The authors declare no conflict of interest.

*This Direct Submission article had a prearranged editor.

¹To whom correspondence should be addressed. E-mail: shryu@stanford.edu.

This article contains supporting information online at www.pnas.org/lookup/suppl/doi:10.1073/pnas.1017171108/-DCSupplemental.

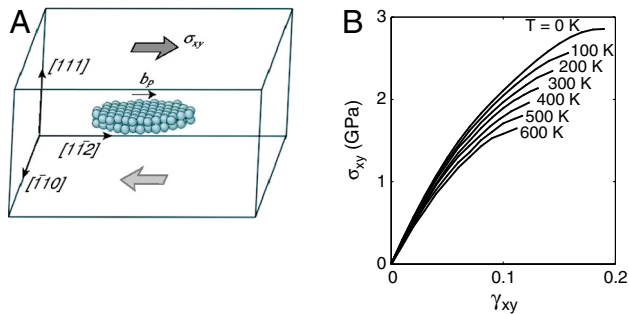


Fig. 1. (A) Schematics of the simulation cell. The spheres represent atoms enclosed by the critical nucleus of a Shockley partial dislocation loop. (B) Shear stress–strain curves of the Cu perfect crystal (before dislocation nucleation) at different temperatures.

umbrella sampling is performed in Monte Carlo simulations using a bias potential as a function of the order parameter n , which is chosen as the number of atoms inside the dislocation loop (*Materials and Methods*).

Fig. 2A shows the free energy function $F(n)$ obtained from umbrella sampling for the specified (T, γ) condition. The maximum of $F(n)$ gives the activation free energy $F_c = 0.53 \pm 0.01$ eV and the critical nucleus size $n_c = 36$. The Zeldovich factor (28), $\Gamma = 0.055$, is obtained from $\Gamma \equiv (\frac{n}{2\pi k_B T})^{1/2}$, where $\eta = -\partial^2 F(n) / \partial n^2|_{n=n_c}$.

Using the configurations collected from umbrella sampling with $n = n_c$ as initial conditions, MD simulations give the attachment rate $f_c^+ = 5.3 \times 10^{14} \text{ s}^{-1}$ (*Materials and Methods*). Because the entire crystal is subjected to uniform stress, the number of nucleation sites is the total number of atoms, $N_{\text{atom}} = 14,976$. Combining these data, the Becker–Döring theory predicts the total nucleation rate to be $N_{\text{atom}} I^{\text{BD}} = 5.5 \times 10^8 \text{ s}^{-1}$, which is within a factor of three of the MD prediction. The difference between the two is comparable to our error bar. This agreement is noteworthy because no adjustable parameters (such as the frequency prefactor) is involved in this comparison. It shows that the Becker–Döring theory and our numerical approach are suitable for the calculation of the dislocation nucleation rate.

We now examine the dislocation nucleation rate under a wide range of temperature and strain (stress) conditions relevant for experiments and beyond the limited timescale of MD simulations. Fig. 3A shows the activation Helmholtz free energy $F_c(T, \gamma)$ as a function of γ at different T . The zero temperature data are obtained with a minimum energy path (MEP) search using a modified version of the string method, similar to that used in refs. 29 and 17. The downward shift of F_c curves with increasing T and is the signature of the shift of activation entropy S_c . Fig. 3C

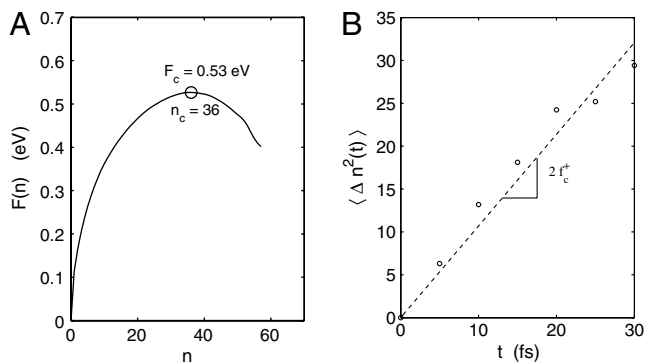


Fig. 2. (A) Free energy of dislocation loop during homogeneous nucleation at $T = 300$ K, $\sigma_{xy} = 2.16$ GPa ($\gamma_{xy} = 0.135$) from umbrella sampling. (B) Size fluctuation of critical nuclei from MD simulations.

plots F_c as a function of T at $\gamma = 0.092$. For $T \leq 400$ K, the data closely follow a straight line, whose slope gives $S_c = 9k_B$. This activation entropy contributes a significant multiplicative factor, $\exp(S_c/k_B) \approx 10^4$, to the absolute nucleation rate, and cannot be ignored.

What causes this rapid drop of activation free energy with temperature? Thermal expansion and vibrational entropy are two candidate mechanisms. To examine the effect of thermal expansion, we performed a zero temperature MEP search at $\gamma = 0.092$, but with other strain components fixed at the equilibrated values at $T = 300$ K. This approach is similar to the quasi-harmonic approximation (QHA) (30, 31) often used in free energy calculations in solids, except that, unlike QHA, the vibrational entropy is completely excluded here. The resulting activation energy, $\bar{E}_c = 2.04$ eV, is indistinguishable from the activation free energy $F_c = 2.05 \pm 0.01$ eV at $T = 300$ K computed from umbrella sampling. Because atoms do not vibrate in the MEP search, this result shows that the dominant mechanism for the large $S_c(\gamma)$ is thermal expansion, whereas the contribution from vibrational entropy is negligible. As temperature increases, thermal expansion pushes neighboring atoms further apart and weakens their mutual interaction. This expansion makes crystallographic planes easier to shear and significantly reduces the free energy barrier for dislocation nucleation. In the widely used harmonic approximation of TST, the activation entropy is often attributed to the vibrational degrees of freedom as $\nu_0 \exp(S_c/k_B) = (\prod_{i=1}^M \nu_i^m) / (\prod_{i=1}^{M-1} \nu_i^a)$, where ν_i^m and ν_i^a are the positive normal frequencies around the local energy minimum and activated state, respectively (5, 18, 32). However, here we see that $S_c(\gamma)$ arises entirely from the anharmonic effect for dislocation nucleation. At $T = 400$ K and $T = 500$ K, we observe significant differences between F_c computed from umbrella sampling and \bar{E}_c computed from MEP search in the expanded cell (*SI Appendix*). These differences must also be attributed to anharmonic effects.

Although it is easier to control strain γ than stress σ in atomistic simulations, it is usually easier to apply stress in experiments, and experimental results are often expressed as a function of σ and T . To bridge between simulations and experiments, it is important to establish a connection between the constant stress and constant strain ensembles. In the constant strain ensemble, the system is described by the Helmholtz free energy $F(n, T, \gamma)$, where n is the size of the dislocation loop and the activation Helmholtz free energy is defined as $F_c(T, \gamma) \equiv F(n_c, T, \gamma) - F(n = 0, T, \gamma)$. In the constant stress ensemble, the system is described by the Gibbs free energy $G(n, T, \sigma)$, from the Legendre transform $G = F - \sigma \gamma V$, with $\sigma \equiv V^{-1} \partial F / \partial \gamma|_{n, T}$. Similarly, $G_c(T, \sigma) \equiv G(n_c, T, \sigma) - G(n = 0, T, \sigma)$. We have proved that $G_c(T, \sigma) = F_c(T, \gamma)$ in the thermodynamic limit of $V \rightarrow \infty$, when σ and γ satisfies the stress–strain relation of the perfect crystal, $\sigma(\gamma, T)$. The difference between F_c and G_c when $\sigma = \sigma(T, \gamma)$ is of the order $\mathcal{O}(V^{-1})$. The details of the proof will be published separately.

Combining the activation Helmholtz free energy $F_c(T, \gamma)$ shown in Fig. 3A and the stress–strain relations shown in Fig. 1B, we obtain the activation Gibbs free energy $G_c(T, \sigma)$, which is shown in Fig. 3B. We immediately notice that the curves at different temperatures are more widely apart in $G_c(T, \sigma)$ than that in $F_c(T, \gamma)$, indicating a much larger activation entropy in the constant stress ensemble. For example, Fig. 3D plots G_c as a function of T at $\sigma = 2.0$ GPa, from which we can obtain an averaged activation entropy of $\bar{S}_c(\sigma) = 48k_B$ in the temperature range of [0, 300 K]. This activation entropy contributes a multiplicative factor of $\exp[\bar{S}_c(\sigma)/k_B] \approx 10^{20}$ to the absolute nucleation rate.

The dramatic difference between $S_c(\gamma)$ and $S_c(\sigma)$ may seem surprising. Indeed, they are sometimes used interchangeably (33, 34), although the conceptual difference between the two has been pointed out in the context of chemical reactions (35, 36).

thermodynamic “compensation law” (37), which states that the activation entropy is proportional to the activation enthalpy (or energy). We find that $S_c(\gamma)$ can be roughly approximated by $E_c(\gamma)/T^*$ with $T^* \approx 3,000$ K, whereas $S_c(\sigma)$ is not proportional to $H_c(\sigma)$ (SI Appendix).

To assess the applicability of these conclusions in heterogeneous nucleation, we studied dislocation nucleation from the corner of a [001]-oriented copper nanorod with {100} side surfaces under axial compression (Materials and Methods). Fig. 4B plots the activation free energy barrier as a function of axial compressive stress σ , which shows significant reduction of the activation free energy with temperature. For example, at the compressive elastic strain of $\epsilon = 0.03$, the compressive stress is $\sigma = 1.50$ GPa at $T = 0$ K. The activation entropy $S_c(\epsilon)$ at this elastic strain equals $9k_B$, whereas the activation entropy $S_c(\sigma)$ at this stress equals $17k_B$. Fig. 4C plots the contour lines of the predicted dislocation nucleation rate (per nucleation site) as a function of T and σ . To show the physical effect of the large activation entropies, the dashed lines plot the rate predictions if the effect of $S_c(\sigma)$ were completely neglected. Significant deviations between the two sets of contour lines are observed, especially for $T \geq 300$ K and $\sigma \leq 1.5$ GPa. For example, at $T = 300$ K and $\sigma = 1.5$ GPa (where a thick and a thin contour line cross), the neglect of activation entropy would cause an underestimate of the nucleation rate by 10 orders of magnitude.

In summary, we have shown that the Becker–Döring theory combined with free energy barriers determined by umbrella sampling can accurately predict the rate of homogeneous dislocation nucleation. In both homogeneous and heterogeneous dislocation nucleation, a large activation entropy at constant elastic strain is observed, and is attributed to the weakening of atomic bonds caused by thermal expansion. An even larger activation entropy is observed at constant stress, caused by thermal softening. Both effects are anharmonic in nature, and emphasize the need to go beyond harmonic approximation in the application of rate theories in solids. We believe our methods and the general conclusions are applicable to a wide range of nucleation processes in solids that are driven by shear stress, including cross slip, twinning, and martensitic phase transformation.

Materials and Methods

Molecular Dynamics. The simulation cell for homogeneous dislocation nucleation has dimension $8[11\bar{2}] \times 6[111] \times 3[1\bar{1}0]$. Periodic boundary conditions (PBC) are applied to all three directions. To reduce artifacts from periodic image interactions, the applied stress is always large enough so that the diameter of the critical dislocation loop is smaller than half the width of the simulation cell.

The shear strain γ is the x - y component of the engineering strain. The following procedure is used to obtain the pure shear stress–strain curve

shown in Fig. 1B. At each temperature T and shear strain γ_{xy} , a series of 2 ps MD simulations under the canonical, constant temperature–constant volume (NVT) ensemble are performed. After each simulation, all strain components except γ_{xy} are adjusted according to the average virial stress until σ_{xy} is the only nonzero stress component. The shear strain is then increased by 0.01 and the process repeats until the crystal collapses spontaneously. The shear stress–strain data are fitted to a polynomial function, $\sigma(\gamma, T) = \sum_{i=0}^2 \sum_{j=0}^2 a_{ij} \gamma^i T^j$ in the range of $0.09 \leq \gamma \leq 0.12$ and $0 \leq T \leq 500$ K.

To obtain average nucleation time at $\sigma_{xy} = 2.16$ GPa ($\gamma = 0.135$) at 300 K, we performed 192 independent MD simulations using the NVT ensemble with random initial velocities. Each simulation ran for 4 ns. If dislocation nucleation occurred during this period, the nucleation time was recorded. This information is used to construct the function $P_s(t)$, which is the fraction of MD simulation cells in which dislocation nucleation has not occurred at time t . $P_s(t)$ can be well fitted to the form of $\exp(-I^{\text{MD}} t)$ to extract the nucleation rate I^{MD} .

To compute the attachment rate f_c^+ , we collected from umbrella sampling an ensemble of 500 atomic configurations for which $n = n_c$, and ran MD simulations using each configuration as an initial condition. The initial velocities are randomized according to Boltzmann’s distribution. The mean square change of the loop size, $\langle \Delta n^2(t) \rangle$, as shown in Fig. 2B, was fitted to a straight line, $2f_c^+ t$, to extract f_c^+ (39).

Free Energy Barrier Calculations. The reaction coordinate n is defined for each atomic configurations in the following way. An atom is labeled as “slipped” if its distance from any of its original nearest neighbors has changed by more than the critical distance d_c (40). We chose $d_c = 0.33, 0.38$, and 0.43 Å for $T \leq 400$ K, $T = 500$ K, and $T = 600$ K, respectively. The slipped atoms were grouped into clusters; two atoms belong to the same cluster if their distance was less than the cutoff distance r_c (3.4 Å). The reaction coordinate n is the number of atoms in the largest cluster divided by two.

To perform umbrella sampling, a bias potential $k_B \hat{T}(n - \bar{n})^2$ is superimposed on the EAM potential, where $\hat{T} = 40$ K and \bar{n} is the center of the sampling window. We chose \hat{T} empirically so that the width of the sampling window on the n -axis would be about 10. The activation Helmholtz free energy data for homogeneous nucleation can be fitted very well by a polynomial function, $F_c(\gamma, T) = \sum_{i=0}^2 \sum_{j=0}^2 b_{ij} \gamma^i T^j$ in the range of $0.09 \leq \gamma \leq 0.12$ and $0 \leq T \leq 500$ K.

For heterogeneous dislocation nucleation, the size of the copper nanorod (17) is $15[100] \times 15[010] \times 20[001]$ with PBC along [001]. The activation Gibbs free energy data for heterogeneous nucleation is fitted to an empirical form $G_c(\sigma, T) = A[(\sigma/\sigma_0)^p - 1]^q - B\sigma T$.

The error bar of activation free energies is about $0.5k_B$. Hence the error bar of activation entropies is about $0.5k_B$.

ACKNOWLEDGMENTS. This work is supported by National Science Foundation Grant CMS-0547681, a Department of Energy Scientific Discovery through Advanced Computing project on Quantum Simulation of Materials and Nanostructures, and the Army High Performance Computing Research Center at Stanford University. S.R. acknowledges support from the Weiland Family Stanford Graduate Fellowship.

- Walsh MR, Koh CA, Sloan ED, Sum AK, Wu DT (2009) Microsecond simulations of spontaneous methane hydrate nucleation and growth. *Science* 326:1095–1098.
- Anderson VJ, Lekkerkerker HNW (2002) Insights into phase transition kinetics from colloid science. *Nature* 416:811–815.
- Matsumoto M, Saito S, Ohmine I (2002) Molecular dynamics simulation of the ice nucleation and growth process leading to water freezing. *Nature* 416:409–413.
- Laaksonen A, Talanquer V, Oxtoby DW (1995) Nucleation: Measurements, theory, and atmospheric applications. *Annu Rev Phys Chem* 46:489–524.
- Hänggi P, Talkner P, Borkovec M (1990) Reaction-rate theory: Fifty years after Kramers. *Rev Mod Phys* 62:251–342.
- ten Wolde PR, Frenkel D (1997) Enhancement of protein crystal nucleation by critical density fluctuations. *Science* 277:1975–1978.
- Izumi S, Ohta H, Takahashi C, Suzuki T, Saka H (2010) Shuffle-set dislocation nucleation in semiconductor silicon device. *Philos Mag Lett* 90:707–714.
- Li X, Wei Y, Lu L, Lu K, Gao H (2010) Dislocation nucleation governed softening and maximum strength in nanotwinned metals. *Nature* 464:877–880.
- Li J (2007) The mechanics and physics of defect nucleation. *MRS Bull* 32:151–159.
- Zhu T, Li J, Ogata S, Yip S (2009) Mechanics of ultra-strength materials. *MRS Bull* 34:167–172.
- Li J, Van Vliet KJ, Zhu T, Yip S, Suresh S (2002) Atomistic mechanisms governing elastic limit and incipient plasticity in crystals. *Nature* 418:307–310.
- Schuh CA, Mason JK, Lund AC (2005) Quantitative insight into dislocation nucleation from high-temperature nanoindentation experiments. *Nat Mater* 4:617–621.
- Schall P, Cohen I, Weitz DA, Spaepen F (2006) Visualizing dislocation nucleation by indenting colloidal crystals. *Nature* 440:319–323.
- Xu G, Argon AS, Ortiz M (1997) Critical configurations for dislocation nucleation from crack tips. *Philos Mag A* 75:341–367.
- Bringa EM, et al. (2006) Shock deformation of face-centered-cubic metals on subnanosecond timescales. *Nat Mater* 5:805–810.
- Tschopp MA, Spearot DE, McDowell DL Atomistic simulations of homogeneous dislocation nucleation in single crystal copper. *Modell Simul Mater Sci Eng* 15:693–709.
- Zhu T, Li J, Samanta A, Leach A, Gall K (2008) Temperature and strain-rate dependence of surface dislocation nucleation. *Phys Rev Lett* 100:025502.
- Vineyard GH (1957) Frequency factors and isotope effects in solid state rate processes. *J Phys Chem Solids* 3:121–127.
- Jónsson H, Mills G, Jacobsen KW (1998) Nudged elastic band method for finding minimum energy paths of transitions. *Classical and Quantum Dynamics in Condensed Phase Simulations*, eds BJ Berne, G Ciccotti, and DF Coker (World Scientific, Singapore), pp 385–404.
- Warner DH, Curtin WA (2009) Origins and implications of temperature-dependent activation energy barriers for dislocation nucleation in face-centered cubic metals. *Acta Mater* 57:4267–4277.
- Frenkel D, Smit B (2002) *Understanding Molecular Simulation: From Algorithms to Applications* (Academic, San Diego).
- Ren WEW, Vanden-Eijnden E (2005) Finite temperature string method for the study of rare events. *J Phys Chem B* 109:6688–6693.

23. Valeriani C, Allen RJ, Morelli MJ, Frankel D, ten Wolde PR (2007) Computing stationary distributions in equilibrium and nonequilibrium systems with forward flux sampling. *J Chem Phys* 127:114109.
24. Becker R, Döring W (1935) The kinetic treatment of nuclear formation in supersaturated vapors. *Ann Phys (Weinheim, Ger)* 24:719–752.
25. Khantha M, Pope DP, Vitek V (1994) Dislocation screening and the brittle-to-ductile transition: A Kosterlitz–Thouless type instability. *Phys Rev Lett* 74:684–687.
26. Mishin Y, Mehl MJ, Papaconstantopoulos DA, Voter AF, Kress JD (2001) Structural stability and lattice defects in copper: Ab initio, tight-binding, and embedded-atom calculations. *Phys Rev B: Condens Matter Mater Phys* 63:224106.
27. Hirth JP, Lothe J (1982) *Theory of Dislocations* (Wiley, New York).
28. Zeldovich YB (1943) On the theory of new phase formation: Cavitation. *Acta Physicochim URSS* 18:1–22.
29. Zhu T, Li J, Samanta A, Kim HG, Suresh S (2007) Interfacial plasticity governs strain rate sensitivity and ductility in nanostructured metals. *Proc Natl Acad Sci USA* 104:3031–3036.
30. Foiles SM (1994) Evaluation of harmonic methods for calculating the free energy of defects in solids. *Phys Rev B: Condens Matter Mater Phys* 49:14930–14938.
31. de Koning M, Miranda Caetano R, Antonelli A (2002) Atomistic prediction of equilibrium vacancy concentrations in Ni₃Al. *Phys Rev B: Condens Matter Mater Phys* 66:104110.
32. Gupta D, ed. (2002) *Diffusion Processes in Advanced Technological Materials* (Williams Andrew Publishing, New York), pp 138–140.
33. Huntington HB, Shinn GA, Wajda ES (1955) Calculation of the entropies of lattice defects. *Phys Rev* 99:1085–1091.
34. DiMelfi RJ, Nix WD, Barnett DM, Holbrook JH, Pound GM (1980) The equivalence of two methods for computing the activation entropy for dislocation motion. *Acta Mater* 28:231–337.
35. Whalley E (1964) Use of volumes of activation for determining reaction mechanisms. *Advances in Physical Organic Chemistry*, ed V Gold (Academic, London), pp 93–162.
36. Tonnet ML, Whalley E (1975) Effect of pressure on the alkaline hydrolysis of ethyl acetate in acetone-water solutions. Parameters of activation at constant volume. *Can J Chem* 53:3414–3418.
37. Kemeny G, Rosenberg B (1973) Compensation law in thermodynamics and thermal death. *Nature* 243:400–401.
38. Li J (2003) AtomEye: An efficient atomistic configuration viewer. *Modell Simul Mater Sci Eng* 11:173–177.
39. Ryu S, Cai W Validity of classical nucleation theory for Ising models. *Phys Rev E: Stat, Nonlinear, Soft Matter Phys* 81:030601(R).
40. Ngan AHW, Zuo L, Wo PC (2006) Size dependence and stochastic nature of yield strength of micron-sized crystals: A case study on Ni₃Al. *Proc R Soc A* 462:1661–1681.